AIAA JOURNAL
Vol. 30, No. 10, October 1992

Experimental and Numerical Investigations of Low-Density Nozzle and Plume Flows of Nitrogen

Iain D. Boyd*
Eloret Institute, Palo Alto, California 94303
Paul F. Penko†
NASA Lewis Research Center, Cleveland, Ohio 44135
and
Dana L. Meissner‡ and Kenneth J. DeWitt§
University of Toledo, Toledo, Ohio 43606

Experimental and numerical investigations are performed and compared for the flow of nitrogen in a small nozzle and in the near field of the plume resulting from expansion into near-vacuum conditions. The experimental data obtained were in the form of pressure measurements using a pitot tube, in the nozzle-exit plane and near field of the plume. Since the flow regimes vary from continuum, at the nozzle throat, to rarefied, in the plume, two different numerical studies are undertaken: the first employs a continuum approach in solving the Navier-Stokes equations, and the second employs a stochastic particle approach through the use of the direct simulation Monte Carlo (DSMC) method. Comparison of the experimental data and the numerical results at the nozzle exit reveals that the DSMC technique provides the more accurate description of the expanding flow. It is discovered that the DSMC solutions are quite sensitive to the model employed to simulate the interaction between the gas and the nozzle-wall surface. It is concluded that the simple fully diffuse model is quite satisfactory for the present application. The study provides the strongest evidence to date that the DSMC technique predicts accurately the flow characteristics of low-density expanding flows.

Nomenclature

D_e = diameter at nozzle exit
D_p = diameter of probe
D_t = diameter at nozzle throat
M_x = Mach number ahead of a shock
P_x = static pressure ahead of a shock
P_o = total pressure
P_{oy} = total pressure behind a shock
P_x = static pressure ahead of a shock
Re_p = probe Reynolds number
T_o = total temperature
T_{ref} = reference temperature
T_w = temperature of nozzle wall
T_x = static temperature ahead of a shock
T_y = static temperature behind a shock
U_o = thermal velocity at total temperature
U_∞ = freestream velocity
γ = ratio of specific heats
μ_{ref} = viscosity given by reference temperature
μ_y = viscosity given by temperature behind a shock
ω = viscosity temperature exponent
ρ_∞ = freestream density

Introduction

FOR the control of satellites and large space structures in orbit, a number of propulsive devices are often used. The thrust level of these engines is usually quite small, and it was thought previously that they presented few problems of integration with the spacecraft. However, as discussed by Dettleff[1] in his excellent review, such rockets may cause a number of deleterious effects which reduce significantly the operational lifetime of a spacecraft. Although the firing times of the thrusters are usually only a few seconds, it must be remembered that they are fired repeatedly for a number of years. This may lead to the gradual accumulation of contamination from the plume on sensitive surfaces such as solar arrays. In addition, the plume can cause heating or electrical charging of the spacecraft, which can alter the thermal balance and damage scientific instruments. Thrust loss and disturbance torques are also unwanted effects which can result from the firing of the control thrusters. The magnitude of these effects is very much dependent on both the thruster design and the satellite configuration.

The assessment of the interaction between the spacecraft and the plume requires an accurate description of the expanding flowfield. Therefore, a research program has been established with the objective of advancing the theoretical predictions of small rocket expansions through comparison with experimental data. The major phenomena to be investigated include the flowfield of low-Reynolds-number nozzles, the resultant plume flowfields and impacts, and the ambient environment effects which arise during testing in ground-based facilities. The approach adopted is to develop and compare various theoretical and numerical techniques used in predictions and to obtain accurate experimental data for code development and verification. Although the program encompasses all low-thrust propulsion concepts, including the neutral flows of resistojets, the plasma flows of arcjet thrusters, and small chemical rockets, the initial emphasis is directed toward an understanding of the nozzle and plume flows of resistojets.

The purpose of the present study is to compare recently acquired experimental data with predictions obtained using numerical methods. The region of study is the nozzle flow, and the near-field expansion of the plume. The gas employed is nitrogen due to its simple diatomic structure. The aim is to

Received Sept. 16, 1991; revision received Jan. 28, 1992; accepted for publication Feb. 6, 1992.

*Research Scientist, mailing address: NASA Ames Research Center, MS 230-2, Moffett Field, CA 94035
†Aerospace Engineer. Member AIAA.
‡Graduate Student, Department of Mechanical Engineering.
§Professor, Department of Chemical Engineering. Member AIAA.

understand the fluid mechanics without complication from other physical processes such as vibrational and chemical nonequilibrium. In this article, description is made of the experimental facility and the type of measurements which have been undertaken at the exit of the nozzle and in the plume. The application of two different numerical techniques is also described. One method provides a continuum analysis from solution of the Navier-Stokes equations. Because of the rarefied nature of the expanding flow, the second method uses a numerical technique that simulates particle behavior at the molecular level, specifically, the direct simulation Monte Carlo (DSMC) method. Although the DSMC method is more numerically intensive than the continuum technique, it is better able to capture a number of potentially important nonequilibrium effects. Previously, it has been found by Boyd and Stark[2] that the DSMC method offers results which yield better correspondence to experimental data in the rarefied flow regime of an expansion plume. In addition, the improper use of continuum methods in the simulation of such plumes can lead to significant underestimation of important impingement characteristics such as heat transfer and drag force.[3] It is therefore an aim of this study to assess any deficiencies in the Navier-Stokes solutions. Particular attention is given to the physical and computational limitations of these methods based on the assumptions inherent to their formulation. This investigation provides the opportunity for assessment of the DSMC technique in modeling an expanding gas. In addition, it will be shown that a portion of the flowfield is particularly sensitive to the model assumptions employed for the interaction between the gas and the surface of the nozzle wall. The coupling of experimental measurements to the computations offers a unique opportunity to investigate the validity of these models.

Reference Problem

For this study, a reference problem was defined that typified the nozzle flow of an electric propulsion device and also matched the flow capacity of the vacuum pumps on the experimental facility. A conical nozzle was selected for both analytical and machining simplicity, but also represents the geometry of a typical small-thruster nozzle. The nozzle for the problem is illustrated in Fig. 1, with details given in Table 1. The nozzle flow conditions are listed in Table 2 for two configurations that correspond to two different experimental apparatus and two slightly different operating conditions.

The nominal Reynolds number of 850, based on throat diameter and the viscosity of the gas at the inlet stagnation temperature, is characteristic of a high-performance resistojet.[4] The nozzle was made sufficiently large to minimize probe size relative to the exit diameter and does not duplicate necessarily in size actual thruster hardware. As previously mentioned, nitrogen was selected as the test gas for analytical convenience and does not represent particularly an actual fluid of spacecraft propulsion system.

Table 1 Nozzle geometry

Inlet diameter D_i	22.1 mm
Throat diameter D_t	3.18 mm
Exit diameter D_e	31.8 mm
Longitudinal radius R_L	3.18 mm
Wall thickness t_w	1.65 mm
Lip thickness t_l	0.25 mm
Inlet half-angle θ_i	45 deg
Exit half-angle θ_i	20 deg
Area ratio $(D_e/D_t)^2$	100

Table 2 Nozzle flow conditions for the two experimental configurations

	Configuration	
	1	2
Total pressure P_o	6400 Pa	6210 Pa
Total temperature T_o	699 K	700 K
Mass flow $\dot{m}$	6.8×10^{-5} kg/s	6.8×10^{-5} kg/s
Reynolds number Re[a]	850	850
Wall temperature T_{w1}	551 K	507 K
Wall temperature T_{w2}	539 K	498 K

[a] $Re = 4\dot{m}/\mu_o D_t$, where μ_o is the gas viscosity at T_o.

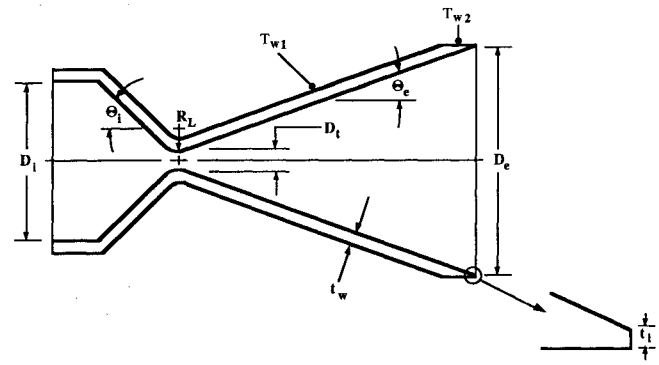

Fig. 1 Nozzle diagram.

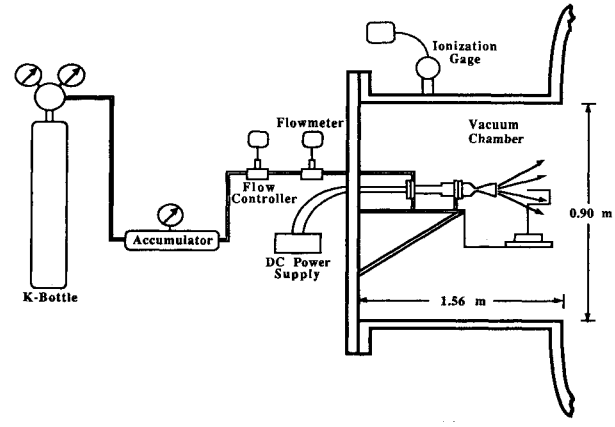

Fig. 2 Schematic of experimental apparatus and test section.

Experimental Investigation

Previous experimental investigations of expanding flow from small rockets include those performed by Bailey[5] with carbon dioxide, and by Legge and Dettleff[5] with hydrazine. The test gases and flow conditions examined in Refs. 5 and 6 made detailed numerical analysis difficult either in terms of physical modeling or computational expense. The present investigation is unique in that the experiment was designed partly on the constraints imposed by the numerical modeling techniques employed in the study. The specific intent was to provide a direct correlation between the model predictions and experimental data.

Test Facility

The experimental tests for this study were conducted in a space-simulation vacuum facility. The experimental apparatus was mounted in a 0.9-m-diam by 1.6-m-long test section that was attached to a tank 4.9 m in diameter and 19 m in length as illustrated in Fig. 2. The vacuum system for the facility consisted of 20 oil-diffusion pumps in series with four blowers and four roughing pumps.[7]

The facility pumping system maintained a vacuum pressure in the test section on the order of 10^{-2} Pa for the nozzle experiments. The vacuum pressure was monitored with a hot-cathode ionization gauge that was mounted on the test section and connected to a digital readout.

Experimental Apparatus

The experimental apparatus for producing the flowfields consisted of a heat exchanger and nozzle (as previously de-

scribed) that simulated a thruster as shown schematically in Fig. 3. Two heat-exchanger assemblies of different design were used in the tests and are illustrated in Figs. 3a and 3b. A traversing mechanism was used to survey the plume with a pressure probe.

In the design illustrated in Fig. 3a, and denoted as configuration 1, the nitrogen was heated in a 3.2-mm-diam tube that was coiled around a cartridge heater of diameter 15.9 mm. In the design illustrated in Fig. 3b, and denoted as configuration 2, the nitrogen was heated in an annular area comprised of a 12.7-mm-diam cartridge heater contained in a tube of 17.3 mm i.d. The heater for configuration 2 had a lower power density and lower surface temperature than that of configuration 1, but the heat exchangers produced the same gas temperature. The design of configuration 2 produced nozzle-wall temperatures about 40 K lower than configuration 1 as listed in Table 2. The heat exchanger on the apparatus was changed from the design of configuration 1 to the design of configuration 2 to lengthen the operational life of the heating element.

For both configurations, the pressure and temperature of the flow were measured upstream of the nozzle in a 22.1-mm-diam plenum. The measurements were effectively nozzle-inlet stagnation conditions as the ratio of area at the measurement station to the throat area was about 48:1. The pressure was measured with a capacitance-manometer transducer having a range of 0–13.3 kPa. Temperature was measured with a half shielded, chromel-alumel thermocouple where the hot junction was located at the centerline of the measurement station. The thermocouple was connected to a digital voltmeter with self-contained, cold-junction compensation. The flow of nitrogen was measured with a transducer of the type that relates thermal changes in a capillary tube to volumnetric flowrate. A schematic of the flow system is shown in Fig. 2.

Although the nozzles for each configuration were machined from the same specifications, the plenum pressures differed slightly for equivalent flowrates and gas temperatures (see Table 2). For a flowrate of 6.8×10^{-5} kg/s and a gas temperature of 700 K, configuration 1 had a plenum pressure of 6400 Pa which was slightly higher than the 6210 Pa of configuration 2. The difference in plenum pressures implied a difference in the throat diameters of about 1% with the throat diameter of configuration 2 being the larger of the two.

The experimental apparatus was designed specifically for making measurements in an expanding flow by use of a traversing mechanism. The mechanism consisted of a rotary-traverse table mounted atop two linear-traverse tables, with travel axes mutually perpendicular to provide radial, axial, and rotational movements. The range of travel was 24 mm in the radial direction (R), 36 mm in the axial direction (Z), and 360 deg in rotation (θ). The tables were positioned manually through mechanical links between the rotary handles on each table and handles outside the vacuum chamber. Position of traverse was monitored by linear-variable-differential transformers (LVDTs) mounted on each of the tables. Output signals from the LVDTs were read on a digital voltmeter.

A pitot tube of 1.02 mm o.d. and 0.15-mm wall thickness was used to measure pressure and flow angle in the nozzle plume. The probe had a 30-deg chamfer on the internal diameter at the tip to form a sharp lip at the leading edge. The pitot tube was attached directly to a capacitance manometer having a range of 0–1.33 kPa and a listed manufacturer's accuracy of 0.1% of full scale to measure the pressure. The manometer was mounted directly on the rotary table. The pitot tube was bent in a U-shape so that the tip was located on the axis of the rotary table as shown schematically in Fig. 3b.

Temperatures of the nozzle wall were measured by two chromel-alumel thermocouples that were tack-welded to the outer wall surface. As shown in Fig. 1, a thermocouple was located about midway between the nozzle throat and exit plane T_{w1}, and another at the exit plane T_{w2}.

Test Procedure

The test section containing the experimental apparatus was first evacuated without gas flow to establish zero settings for the capacitance manometers. The vacuum pressure without flow was about 10^{-4} Pa which served as the zero-reference pressure. The flowmeter was zeroed while containing nitrogen at the accumulator supply pressure. After the instruments were zeroed, flow was established in the apparatus and maintained by the flow controller. Simultaneously, 70 V at about 0.9 A was applied to the cartridge heater and time allowed for the system to equilibrate at a nozzle-inlet temperature of 700 K.

After the system reached steady state, pressure scans were made by moving the pitot probe to a given location and then rotating the probe to determine the point of maximum pressure. Following Bailey,[5] the maximum pressure was taken as the pitot pressure reading for the particular location. The angle θ through which the probe was rotated to obtain the maximum pressure was taken as the flow-angle reading. A typical rotary scan, in this case at the exit plane ($Z/D_e = 0$) and a radial position, $R/D_e = 0.38$, is shown in Fig. 4. The flow angles were measured with respect to the nozzle axis. The error in the pressure measurement was estimated to be ± 5 Pa, and in the flow angle, ± 2 deg.

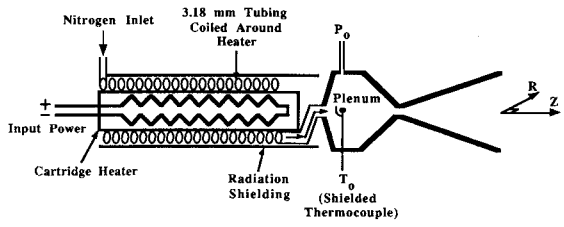

Fig. 3a Hardware schematic of configuration 1.

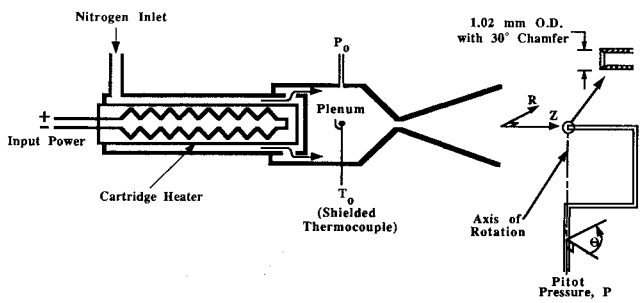

Fig. 3b Hardware schematic of configuration 2.

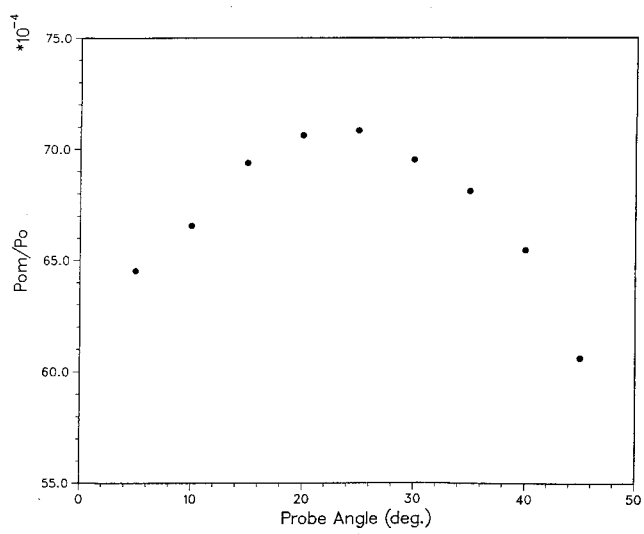

Fig. 4 Measured pitot pressure vs probe angle at $Z = 0$ mm and $R = 12$ mm.

Comparisons of vertical and horizontal scans of pressure across the nozzle diameter indicated that the flow was symmetrical within experimental error. All reported pressure scans were made in the horizontal plane starting at the nozzle centerline ($R/D_e = 0$) and extending outward radially.

Numerical Investigations

Previous numerical investigations of expanding flowfields under rarefied conditions include those of Boyd and Stark,[2,3] Campbell,[8] and Nelson and Doo.[9] Each of the studies employed the DSMC technique, and Refs. 2, 3, and 9 also considered continuum methods, but all were unsatisfactory in different ways. For the different cases, the high computational time requirements of DSMC resulted in the analysis of only a small part of the expansion, in the analysis of an unrealistic thruster configuration, or in the use of numerical parameters that called into question the validity of the computations. As will be discussed in the following sections, the present investigation has the advantage of using a numerically efficient DSMC code which permits the computation of a real nozzle and plume flow without violating numerical restrictions. Another important aspect of the study is the availability of a continuum code which is discussed next.

Continuum Computations

The continuum computation of the flow was made with the numerical code termed the viscous nozzle analysis program (VNAP2) that was originally developed for laminar, viscous nozzle flow.[10] It was later modified to allow computation of both internal and external flows, and, with the inclusion of turbulence models, validated at higher Reynolds number.[11] The code solves the Navier-Stokes equations for a compressible fluid in time-dependent, nonconservative form by the explicit, two-step MacCormack method which gives second-order accuracy in space. With this scheme, the equations are marched in space and iterated in time from a specified initial flowfield to a steady-state solution. For this problem, given the relatively low Reynolds number, laminar flow was assumed.

The code produces a body-fitted, nonorthogonal grid in physical coordinates that, by transformation, is rectangular in computational space. For the problem in this study, 31 radial and 51 axial grid lines were specified. Furthermore, the grid was clustered in the nozzle throat and near the nozzle wall to capture adequately the steep gradients of the flow variables in those regions.

The computation was started in the upstream, subsonic portion of the nozzle. The inflow conditions included specification of total pressure and temperature, and zero radial velocity. The subsonic inflow boundary employed the method of characteristics such that the axial velocity was determined from interior, downstream points, and evolved with the solution from an initial profile.

The stream pressure at the outflow surface in the subsonic portion of the flow was extrapolated rather than specified as is normally done with the code. This scheme gave relatively smooth profiles of properties in the vicinity of the wall at the exit plane, but did, in effect, impose an ambient pressure on the flow. In cases where the subsonic exit-plane pressure was explicitly fixed, the computed properties exhibited a discontinuity across the sonic line where the flow decelerates from supersonic to subsonic in the plane normal to the wall.

The code was iterated for 20,000 timesteps from an initial condition corresponding to one-dimensional, isentropic flow. Convergence of the scheme was not monitored as such, but conservation of mass was checked and used as a guide. At 20,000 timesteps the mass flow was fairly consistent throughout the nozzle. In the diverging section, it was within 1% of the value specified by the inlet conditions, and in the converging section, within 2%.

It is well established that the Navier-Stokes equations break down at high Knudsen numbers due to the failure of the linear forms of the constitutive relations for viscous stress and heat transfer. This problem has received detailed investigation in a study relating to the problem of the normal shock wave.[12] It has been shown that solutions of shock waves obtained with the Navier-Stokes equations give much poorer correspondence to experimental data than computations performed with the DSMC technique, or with the Burnett equations (a higher-order extension of the Navier-Stokes equations). Although Ref. 3 makes direct comparison between DSMC results and a solution of the Euler equations (using the method of characteristics) for an expanding gas under rarefied flow conditions, no such study has been performed previously to investigate the effect of the failure of the Navier-Stokes equations. This was one of the primary aims of the present study.

DSMC Computations

The DSMC method[13] is now a familiar tool employed in the numerical modeling of flows involving rarefied gases. It has been applied to expanding flows in a number of studies, although almost none of these have made direct comparison with experimental data. The present study therefore makes an important contribution in that numerical and experimental studies of an expanding flow have been performed simultaneously. The DSMC code employed in the present work is effectively structured for optimum use on vector supercomputers, and has been described in detail previously.[14] The flow is modeled axisymmetrically in two dimensions using the procedures described in Chapter 9 of Ref. 13.

The code has been configured specifically to compute the flow in the nozzle, in the plume forward of the nozzle, and in a small portion of the backflow. This region has been designed to include a larger area than that investigated experimentally, and to ensure that all flow contributing to that region has been included. It is not, however, the purpose of this study to provide a definitive computation of the backflow region. This would be performed in a more numerically efficient way by starting a fresh computation at the nozzle-exit plane, using the macroscopic results from the present study. This is proposed as a topic worthy of future investigation. The computational domain extends to an axial distance of about 40 mm from the nozzle-exit plane, and to a radial distance of 50 mm. A computational grid of 760×50 nonuniform cells was required to meet the restriction of a cell length of one local mean-free path in the flow direction. The DSMC computations are started at a point just after the nozzle throat using the input of macroscopic properties from the continuum solution. Several different gas/surface interaction models have been considered including specular reflection, diffuse reflection, varying fractions of these two extremes, and the Cercignani-Lampis model implemented in DSMC by Lord.[15] This model offers separate accommodation coefficients for the reflection of the normal and tangential velocity components, and would therefore appear to offer greater versatility than combinations of the diffuse and specular models. For nitrogen, the rotational energy exchange model of Boyd[16] was employed which in essence varies the rotational collision number with temperature. The exchange of vibrational energy is assumed frozen due to the low temperatures encountered in the flowfield.

The limitations of the DSMC technique applied under the present conditions are more of a computational nature, and quite different from the physical difficulties experienced by the Navier-Stokes equations. The numerical cost of DSMC computations is linearly proportional to the density of the flow. This is because the size of a computational cell should be scaled with the mean-free path, which is, of course, itself scaled inversely with the density. Therefore, a high-density flowfield requires a large number of computational cells. This means that more particles must be simulated, and consequently more collisions computed. The computations of the nozzle flow are quite expensive for the DSMC code because the conditions near the nozzle throat are those of a relatively high-density, continuum regime. This computation represents

one of the most numerically intensive simulations undertaken with the DSMC technique. Reasonable computational execution times have been achieved through the vectorization of many parts of the algorithm for efficient performance on a Cray-Y/MP supercomputer.

Calculation of Pitot Pressure

To compare the numerical solutions with experimental data, pitot pressures were first calculated from the numerical results using the computed state variables. The calculated pitot pressure can be viewed as the pressure that would be measured if a pitot tube were inserted into the stream computed by the numerical codes. Since the flow was both supersonic and rarefied, the calculation involved a two-step process:

1) The pressure ratio across a normal shock was calculated with the Rayleigh pitot tube equation (c.f. Ref. 17, p. 154) represented by the functional relation:

$$P_{oy}/P_x = f(\gamma, M_x^2) \tag{1}$$

where γ is the ratio of specific heats which for nitrogen is 1.4.

2) The ideal pressure P_{oy} was corrected for rarefaction effects by

$$\log (P_{om}/P_{oy}) = 0.089 - 0.120 \log (Re_p) \tag{2}$$

This expression is employed for $Re_p \leq 5.6$, otherwise

$$P_{om}/P_{oy} = 1.0$$

where P_{om} is the corrected total pressure behind the shock. The correction in Eq. (2) was obtained from a report on the rarefaction effects of pitot tubes for measuring pressure in rarefied, supersonic, wind-tunnel flow.[18] In Ref. 18, the factor $P_{om}/P_{oy} \geq 1$ was plotted as a function of Re_p, with total temperature of the stream T_o as parameter. Equation (2) is a fit of an interpolated curve for $T_o = 700$ K.

In Ref. 18, the probe Reynolds number was defined as

$$Re_p = \rho_\infty U_\infty D_p/\mu_y \tag{3}$$

In the probe Reynolds number, the actual diameter of the pitot tube on the experimental apparatus was used for D_p. The values of ρ_∞ and U_∞ were obtained from the DSMC results.

The viscosity μ_y was derived from the numerical results by first calculating the temperature behind a shock T_y. This quantity was computed from the normal-shock equation for the ratio of static temperature (c.f. Ref. 17, p. 118) represented by the functional relation

$$T_y/T_x = g(\gamma, M_x^2) \tag{4}$$

where the values of static temperature ahead of the shock T_x and the Mach number M_x were obtained from the numerical results. The viscosity was then found from the standard temperature power-law for the viscosity of gases (c.f. Ref. 19, p. 28):

$$\mu_y = \mu_{\text{ref}} (T_y/T_{\text{ref}})^\omega \tag{5}$$

where μ_{ref} was taken[20] as 2.58×10^{-5} N – s/m^2, the viscosity of nitrogen at the reference temperature T_{ref} of 500 K, and ω was 0.75.

Results and Discussion

The continuum code was executed using the input of Tables 1 and 2. The wall temperature distribution was estimated from the values obtained experimentally with the thermocouples, and was employed in both the continuum and DSMC computations. The continuum solution near the nozzle throat was then employed to obtain a solution of the nozzle flow and the near-field expansion region with the vectorized DSMC code. This procedure was performed for each of the two different experimental configurations. The DSMC code has a numerical efficiency of 1.1×10^{-6} CPU s/timestep/particle, and the computation required 3 CPU h on the Cray Y/MP. The execution time for the continuum code was 0.8 CPU h.

The first comparison of the two numerical solutions is made in Fig. 5 in which the velocity profiles close to the nozzle throat are shown. Radial distance R and the velocity U have been normalized by the throat diameter D_t and the thermal velocity in the stagnation chamber U_o. Excellent agreement is obtained for the two profiles, verifying that the continuum and DSMC solutions are in agreement in the continuum-flow regime near the nozzle throat.

Significant differences were, however, observed in the two numerical solutions further downstream in the nozzle. In Fig. 6, the velocity profiles computed by the two methods are compared at the nozzle exit plane (the radial distance is hereafter normalized by the nozzle exit diameter D_e). The velocity predicted by DSMC is always greater than the continuum data. It is of particular importance to note that the velocity given by DSMC at the nozzle wall is nonzero. This indicates that the no-slip boundary conditions normally employed in continuum computations are insufficient for this application. The slip effect in rarefied flows is an established phenomenon and is important in the present study due to its significant effect on the boundary-layer thickness. A further comparison at the nozzle-exit plane is shown in Fig. 7 where temperature

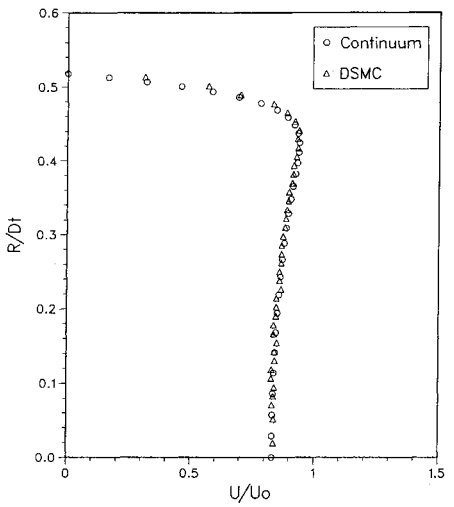

Fig. 5 Comparison of computed velocity profiles at the inflow surface of the DSMC computational domain.

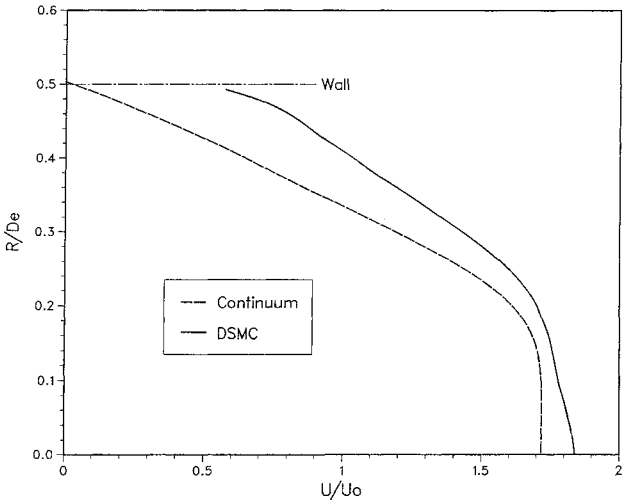

Fig. 6 Comparison of computed velocity profiles in the nozzle-exit plane for configuration 1.

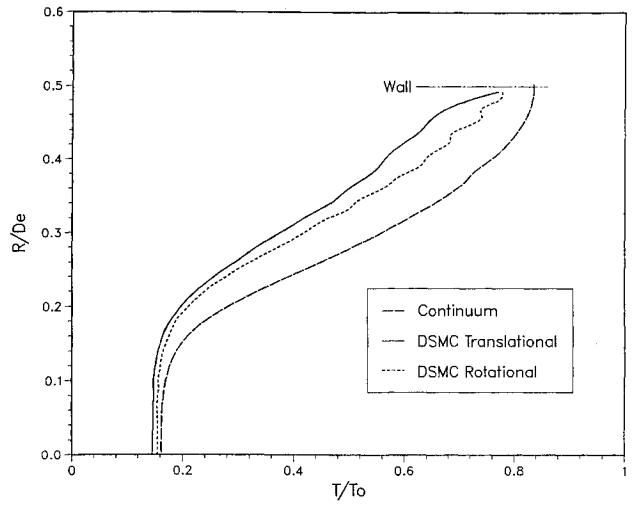

Fig. 7 Comparison of computed temperature profiles in the nozzle-exit plane for configuration 1.

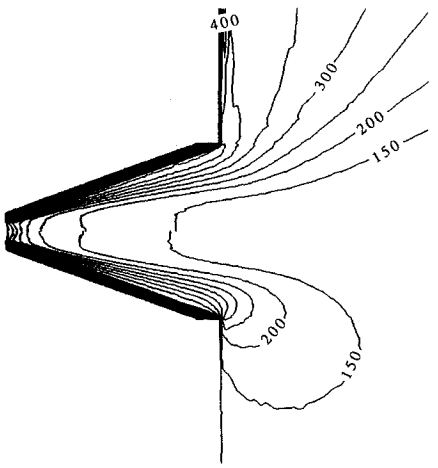

Fig. 8 Comparison of temperature contours computed with DSMC for the translational (lower) and rotational (upper) energy modes.

profiles are shown. Both translational and rotational temperatures are obtained from DSMC, whereas the continuum method, predicated on thermal equilibrium, gives just one temperature. All temperatures are normalized to the stagnation value *To*. The continuum temperature is always higher than both the DSMC temperatures. These latter values show only a small degree of nonequilibrium in the low-density region close to the nozzle wall.

The nonequilibrium between the modes of translational and rotational energy is more accentuated as the plume expands away from the nozzle. This phenomenon is observed clearly in Fig. 8 where the translational temperature, shown in the lower portion of the figure, is compared with the rotational temperature, shown in the upper portion. At the nozzle lip, the translational temperature is turned into the lip, and seems to curve around the blunt end of the wall. By comparison, the rotational temperature freezes quite quickly in this region, due to the relatively low density. The vertical lines from the nozzle lip in Fig. 8 indicate a plane beyond which excessive statistical scatter exists in the computed data. As stated earlier, the backflow region of the flow will be computed in the future with a separate simulation to be begun at the nozzle-exit plane.

The structure of the nozzle and plume flow computed with the DSMC method is further considered in Fig. 9 where contours of Mach number (lower portion) and flow angle (upper portion) are shown. The Mach number contours reveal that the sonic line intersects the nozzle lip, as observed previously by Bird.[21] Although not shown here, comparison with the continuum data revealed that the solutions for Mach number agreed in the near-continuum flow regime near the nozzle throat. Proceeding further down the nozzle, however, showed the Mach numbers computed with DSMC becoming increasingly larger than the corresponding continuum values. Careful examination of the flow-angle data reveals that the flow near the lip in the nozzle-exit plane is turned up towards the wall. In this region, the flow-angle becomes greater than the nozzle half-angle of 20 deg. This behavior was also observed in the study by Campbell.[8] As the gas expands further out away from the nozzle, the flow-angle data begins to resemble the flow from a point source.

In Fig. 10, the pitot pressure profiles in the nozzle-exit plane are shown for configuration 1 (pitot pressure, P_{om}, has been normalized by the stagnation pressure *Po*). Four separate profiles are shown: the experimental data, the continuum solution, and two DSMC solutions employing two different gas/surface interaction models. The DSMC computation which employs fully diffuse reflection at the wall gives the best correspondence to the experimental data. The continuum solution predicts higher pitot pressures in the isentropic core of the expansion, and then lower pressures in the thick, laminar boundary layer. The DSMC solution employing specular wall reflection essentially provides a nonviscous Euler solution with no boundary layer. The sensitivity of the exit-plane profile to the surface model is readily seen by comparison of the

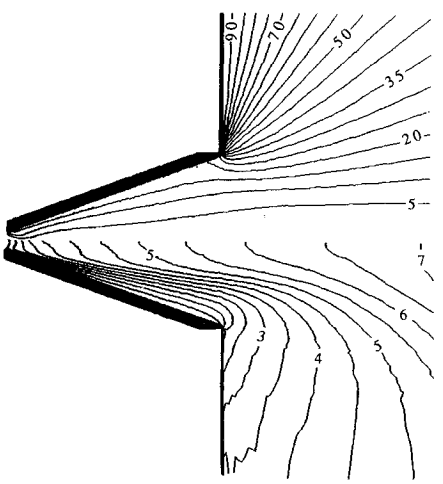

Fig. 9 Mach number (lower) and flow angle (upper) contours computed with DSMC.

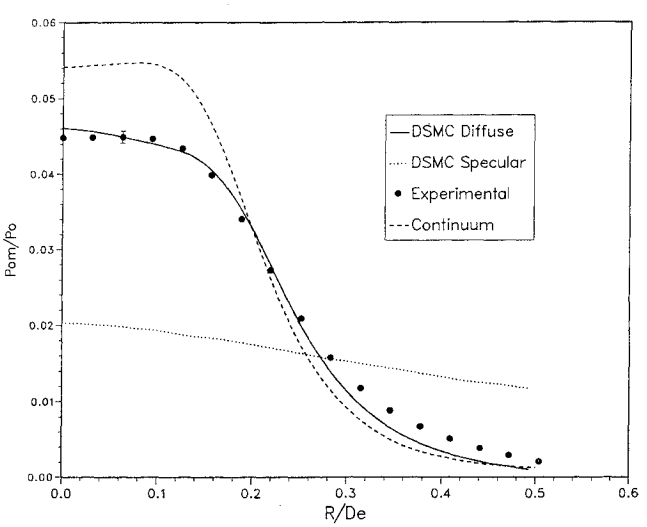

Fig. 10 Comparison of computed (DSMC and continuum) and measured pitot pressure profiles for configuration 1 in the nozzle-exit plane at $Z = 0$ mm.

two DSMC solutions. Further DSMC computations employing varying combinations of diffuse and specular reflection, and the Cercignani-Lampis model,[15] all gave profiles lying between the two extremes indicated in Fig. 10. The fact that the diffuse model agrees so well with the experimental data is a strong indication that this model is well suited to the subsonic flow along the nozzle wall. This study provides one of the very rare occasions in which gas/surface interaction models for the DSMC technique have been assessed directly through comparison with experimental flowfield data. The sensitivity of the computations to the wall model indicates that possibilities exist for the assessment of such phenomena through carefully designed experiments, without recourse to molecular-beam studies.

It is difficult to ascertain whether the differences between the continuum and particle simulation results are due to the failure of the Navier-Stokes equations in a rarefied expanding flow, or instead to the no-slip, nozzle-wall boundary condition employed in the continuum analysis and the outflow boundary condition. A computation in Ref. 13 (p. 188) proposes that the translational temperature is lower than the continuum temperature, and the rotational temperature higher, for a one-dimensional steady spherical expansion at a similar Knudsen number as the nozzle flow. The exact divergence of the translational and rotational temperatures is very much dependent upon the

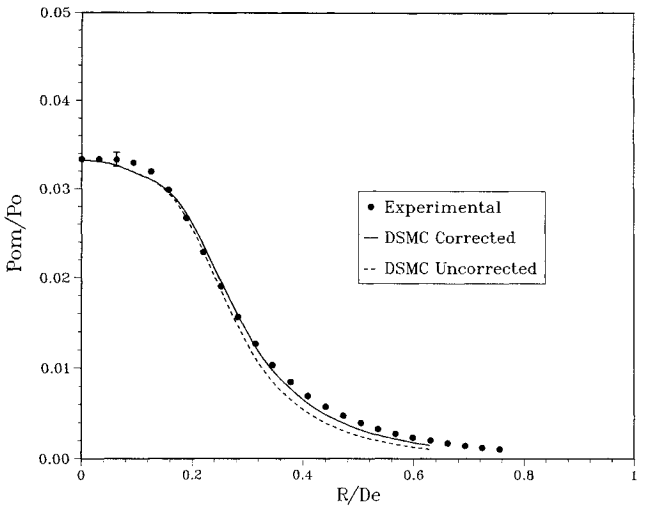

Fig. 11 Comparison of computed (DSMC) and measured pitot pressure profiles for configuration 1 at $Z = 12$ mm.

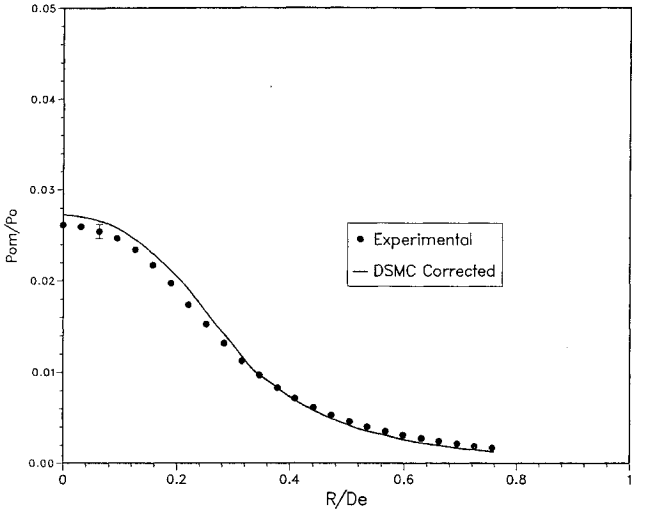

Fig. 12 Comparison of computed (DSMC) and measured pitot pressure profiles for configuration 1 at $Z = 24$ mm.

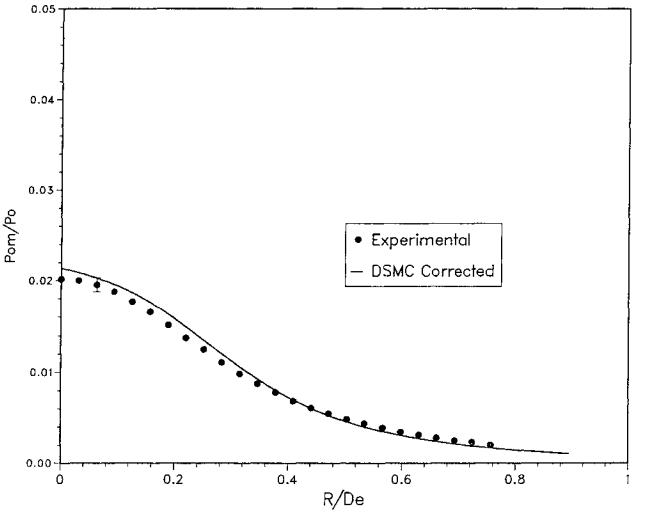

Fig. 13 Comparison of computed (DSMC) and measured pitot pressure profiles for configuration 1 at $Z = 36$ mm.

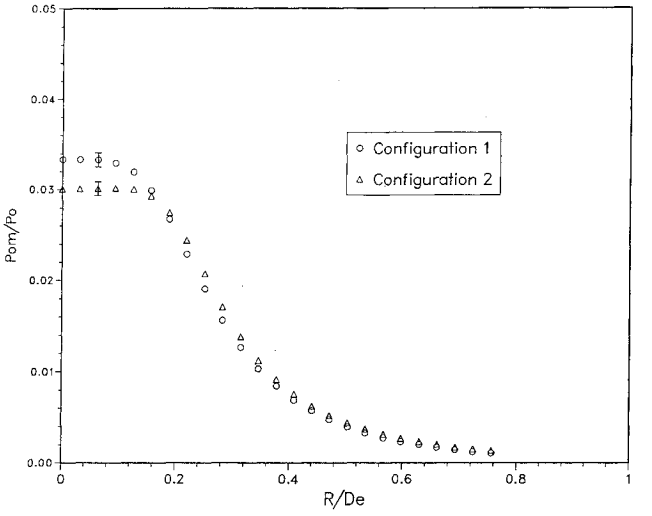

Fig. 14 Comparison of measured pitot pressure profiles for configurations 1 and 2 at $Z = 12$ mm.

rotational-energy-exchange model employed in the simulation. The two models used in Ref. 13 are different from that employed in the present study. Also, the present application is complicated by two-dimensional and boundary-layer effects. However, it is reasonable to expect similar nonequilibrium behavior as that which occurs in the one-dimensional, steady expansion. Therefore, it is concluded that the continuum computation does not predict the flow correctly because of its inability to capture thermal-nonequilibrium effects and the requirement for use of a slip boundary condition (both of which are recognized deficiencies of the Navier-Stokes equations applied to rarefied flows).

In Fig. 11, the pitot pressure profiles at an axial distance of 12 mm from the nozzle-exit plane are shown for experimental configuration 1. The two profiles obtained with the DSMC technique show the effect of applying the correction of Eq. (2) to the computed results. Once again, the DSMC solutions give excellent correspondence to the experimental data. These same trends are observed further downstream at distances of 24 and 36 mm from the nozzle-exit plane in Figs. 12 and 13. It is most encouraging to find that the excellent agreement between the DSMC computations and the experimental data is continued into the plume where the correction factors employed in Eq. (2) become larger as the density, and the probe Reynolds number, decrease. Although the data from Ref. 17 used for the corrections has been corroborated to some extent by the

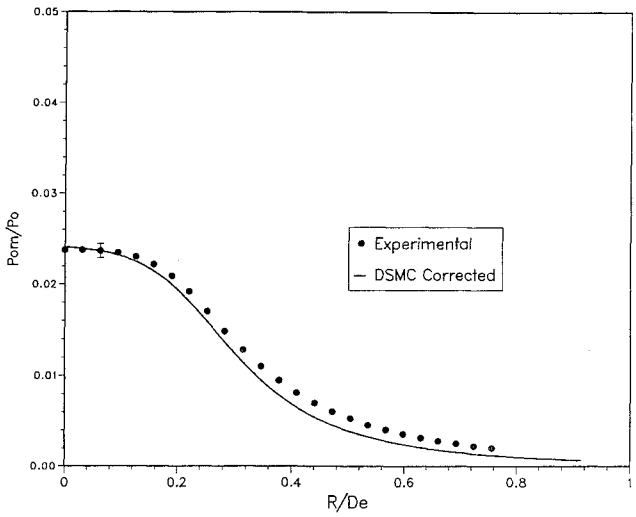

Fig. 15 Comparison of computed (DSMC) and measured pitot pressure profiles for configuration 2 at $Z = 24$ mm.

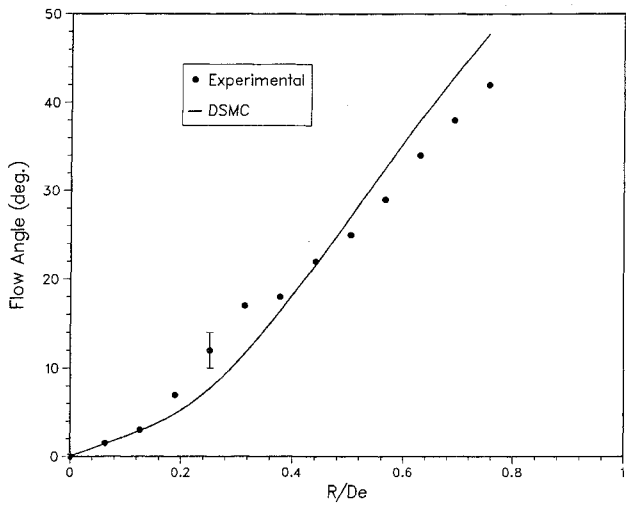

Fig. 16 Comparison of computed (DSMC) and measured flow angle for configuration 2 at $Z = 12$ mm.

experimental data taken in the present study, the Reynolds numbers reached in Fig. 13 were right at the lower limit of that study. It is the intention to investigate these effects thoroughly in the future with the DSMC method.

The effect of the two different experimental apparatus is now considered. Radial scans of pitot pressure for both experimental configurations, at an axial distance of 12 mm from the nozzle exit, are shown in Fig. 14. The pressures from configuration 2 (triangular symbol) are lower in the core of the flow near the centerline, and the overall profile flatter than those for configuration 1 (circular symbol). The pressures from both configurations are nearly the same in the outer region of the plume. This figure is typical of the difference in pressure profiles between the two experimental configurations. A comparison of the DSMC results computed for configuration 2, at an axial distance of 24 mm from the nozzle exit, is shown in Fig. 15. Once again, the numerical data offers excellent agreement with the experiment. It is significant that the DSMC computations have been successful in predicting the lower pressure at the centerline and the flatter profile observed experimentally for configuration 2.

The measurement of pitot pressure at locations away from the plume axis involves rotation of the probe. As explained earlier, the experimental data is recorded as the maximum pressure obtained during this rotation. This point also provides the angle of the flow at each location in the flowfield. An example of this data is shown in Fig. 16 for configuration 2 at the location of 12 mm from the nozzle exit plane. It is found that the DSMC computations offer fairly good agreement with the probe measurements, except in the vicinity of $R/D_e = 0.31$, where the measurements exhibited some scatter. It is the aim in the future to improve our confidence in the flow-angle measurements through use of a conical probe designed specifically for this task. The comparison between experiment and DSMC analysis for flow angle further demonstrates the capability of the numerical technique.

Concluding Remarks

By comparison with new experimental data, it has been shown that the direct simulation Monte Carlo method provides an accurate description of a low-density flow in the nozzle and the near-field expansion of a small rocket for two slightly different experimental configurations. This study thereby provides verification of the DSMC method in an expanding flow for the first time. From a number of different gas/surface interaction models, it was found that fully diffuse reflection gave the best agreement with experiment. Solutions of the Navier-Stokes equations under the same conditions were less successful in predicting the flow correctly. It is well established that, for rarefied flows, the Knudsen number becomes so great that the assumptions invoked in developing the Navier-Stokes equations are invalidated. In previous studies of shock waves, it has been shown that the DSMC technique offers better correspondence to experimental data under conditions where the Navier-Stokes equations break down. It is therefore concluded that the failure of the continuum solution is affected by the physical limitations of the Navier-Stokes equations. This is made worse in the present study because low-density, slip effects along the nozzle wall are also important.

Acknowledgment

Support for the first author by NASA Grant NCC2-582 is gratefully acknowledged.

References

[1]Dettleff, G., "Plume Flow and Plume Impingement in Space Technology," *Progress in Aerospace Science*, Vol. 28, 1991, pp. 1–71.

[2]Boyd, I. D., and Stark, J. P. W., "Modeling of a Small Hydrazine Thruster Plume in the Transition Flow Regime," *Journal of Propulsion and Power*, Vol. 6, No. 2, 1990, pp. 121–126.

[3]Boyd, I. D., and Stark, J. P. W., "Assessment of Impingement Effects in the Isentropic Core of a Small Satellite Control Thruster Plume," *Proceedings of the Institution of Mechanical Engineers*, Vol. 203, 1989, pp. 97–103.

[4]Yoshida, R. Y., Halbach, C. R., and Hill, S. C., "Life Test Summary and High Vacuum Tests of 10m lb Resistojets," *Journal of Spacecraft and Rockets*, Vol. 8, No. 4, 1971, pp. 414–416.

[5]Bailey, A. B., "Flow-Angle Measurements in a Rarefied Nozzle Plume," *AIAA Journal*, Vol. 25, No. 12, 1987, pp. 1301–1304.

[6]Legge, H., and Dettleff, G., "Pitot Pressure and Heat Transfer Measurements in Hydrazine Thruster Plumes," *Journal of Spacecraft and Rockets*, Vol. 23, No. 4, 1986, pp. 357–362.

[7]Finke, R. C., Holmes, A. D., and Keller, T. A., "Space Environment Facility for Electric Propulsion Systems Research," NASA TN-D-2774, May 1965.

[8]Campbell, D. H., "Angular Variation of Flowfield Properties in Free Jet Expansions," *Rarefied Gas Dynamics*, edited by A. E. Beylich, VCH Press, Weinheim, Germany, 1991, pp. 1019–1024.

[9]Nelson, D. A., and Doo, Y. C., "Simulation of Multicomponent Nozzle Flows into a Vacuum," *Rarefied Gas Dynamics*, edited by E. P. Muntz, D. P. Weaver, and D. H. Campbell, AIAA, Washington, DC, 1989, pp. 340–351.

[10]Cline, M. C., "Computation of Two-Dimensional, Viscous Nozzle Flow," *AIAA Journal*, Vol. 14, No. 3, 1976, pp. 295–296.

[11]Cline, M. C., and Wilmoth, R. G., "Computation of High Reynolds Number Internal/External Flows," *AIAA Journal*, Vol. 21, No. 2, 1983, pp. 172–173.

[12]Lumpkin, F. E., and Chapman, D. R., "Accuracy of the Burnett Equations for Hypersonic Real Gas Flows," *Journal of Thermo-*

physics and Heat Transfer (to be published); see also AIAA Paper 91-0771, Jan. 1991.

[13]Bird, G. A., *Molecular Gas Dynamics*, Clarendon Press, Oxford, England, UK, 19786.

[14]Boyd, I. D., "Vectorization of a Monte Carlo Method For Nonequilibrium Gas Dynamics," *Journal of Computational Physics*, Vol. 96, Oct. 1991, pp. 411–427.

[15]Lord, R. G., "Application of the Cercignani-Lampis Scattering Kernel to Direct Simulation Monte Carlo Calculations," *Rarefied Gas Dynamics*, edited by A. E. Beylich, VCH Press, Weinheim, Germany, 1991, pp. 1427–1433.

[16]Boyd, I. D., "Analysis of Rotational Nonequilibrium in Standing Shock Waves of Nitrogen," *AIAA Journal*, Vol. 28, No. 11, 1990, pp. 1997–1999.

[17]Shapiro, A. H., *The Dynamics and Thermodynamics of Compressible Fluid Flow*, Ronald Press, New York, 1953.

[18]Stephenson, W. B., "Use of the Pitot Tube in Very Low Density Flows," Arnold Engineering Development Center, Rept. AEDC-TR-81-11, Arnold, AFS, TN, Oct. 1981.

[19]White, F. M., *Viscous Fluid Flow*, McGraw-Hill, New York, 1974.

[20]Vargartik, N. B., *Tables on the Thermophysical Properties of Liquids and Gases*, Wiley, New York, 1975, p. 459.

[21]Bird, G. A., "The Nozzle Lip Problem," *Proceedings of the 9th International Symposium on Rarefied Gas Dynamics*, Vol. I, DFVLR Press, Porz-Wahn, Germany, 1974, pp. A22 1–8.